Accepted Manuscript

Localised delivery of doxorubicin to prostate cancer cells through a PSMA-targeted hyperbranched polymer theranostic

Amanda K. Pearce, Joshua D. Simpson, Nicholas L. Fletcher, Zachary H. Houston, Adrian V. Fuchs, Pamela J. Russell, Andrew K. Whittaker, Kristofer J. Thurecht

PII: S0142-9612(17)30454-4

DOI: 10.1016/j.biomaterials.2017.07.004

Reference: JBMT 18167

To appear in: *Biomaterials*

Received Date: 19 April 2017

Revised Date: 29 June 2017

Accepted Date: 4 July 2017

Please cite this article as: Pearce AK, Simpson JD, Fletcher NL, Houston ZH, Fuchs AV, Russell PJ, Whittaker AK, Thurecht KJ, Localised delivery of doxorubicin to prostate cancer cells through a PSMA-targeted hyperbranched polymer theranostic, *Biomaterials* (2017), doi: 10.1016/j.biomaterials.2017.07.004.

Localised delivery of doxorubicin to prostate cancer cells through a PSMA-targeted hyperbranched polymer theranostic

Amanda K. Pearce[a,b], Joshua D. Simpson[a,b], Nicholas L. Fletcher[a,b], Zachary H. Houston[a,b], Adrian V. Fuchs[a,b], Pamela J. Russell[d], Andrew K. Whittaker[a,b,c] and Kristofer J. Thurecht[a,b,c]*

Abstract

The therapeutic potential of hyperbranched polymers targeted to prostate cancer and loaded with doxorubicin was investigated. Polyethylene glycol hyperbranched polymers were synthesised via RAFT polymerisation to feature glutamate urea targeting ligands for PSMA on the periphery. The chemotherapeutic, doxorubicin, was attached to the hyperbranched polymers through hydrazone formation, which allowed controlled release of the drug from the polymers in in vitro endosomal conditions, with 90 % release of the drug over 36 hours. The polymers were able to target to PSMA-expressing prostate cancer cells in vitro, and demonstrated comparable cytotoxicity to free doxorubicin. The ability of the hyperbranched polymers to specifically facilitate transport of loaded doxorubicin into the cells was confirmed using live cell confocal imaging, which demonstrated that the drug was able to travel with the polymer into cells by receptor mediated internalisation, and subsequently be released into the nucleus following hydrazone degradation. Finally, the ability of the complex to induce a therapeutic effect on prostate cancer cells was investigated through a long term tumour regression study, which confirmed that the DOX-loaded polymers were able to significantly reduce the volume of subcutaneous prostate tumours in vivo in comparison to free doxorubicin and a polymer control, with no adverse toxicity to the animals. This work therefore demonstrates the potential of a hyperbranched polymer system to be utilised for prostate cancer theranostics.

Introduction

Prostate cancer remains a worldwide health concern, with over 600,000 cases and 200,000 men dying annually around the world.[1, 2] Early stage prostate cancer typically has favourable outcomes, with a high rate of successful treatment and promising 5-year survival rates. However, late-stage prostate cancer has a significantly reduced prognosis due to a combination of many factors, including low specificity treatments in the clinic, a limited ability to diagnose in the early stages and complications related to advanced, metastatic occurrences of the disease, where the cancer has spread from the original disease site to other areas of the body.[3-8] The ability to efficiently target disease sites while simultaneously delivering treatment and diagnostic capabilities is the next crucial step towards improving on these outcomes.

Current treatments in the clinic are predominantly systemically administered chemotherapeutic drugs, external radiation and surgery.[9] While these treatments are successful in some cases, they are typically ineffective once the cancer reaches a metastatic castrate resistant stage. In the case of chemotherapeutic drugs that are delivered systemically, the toxicity to normal rapidly dividing cells such as red blood cells and immune cells is a significant problem.[10] Additionally, the poor bioavailability of most chemotherapeutics imparts a significant limitation on the dose that can be delivered to the site of interest, and can negatively impact on the efficacy of the treatment through reduced tumour site localisation.[11, 12] However, the advantage of chemotherapy is that it is able to distribute throughout the body to treat tumours in multiple locations, whereas surgical and radiation approaches are confined to treating one area. Therefore, while both surgery and radiation can be highly effective for singular, large tumour masses, they are extremely inefficient techniques for treating metastatic cancer, and thus there remains a lack of treatment options that are both highly specific and effective for multiple tumour masses.[13] In order to overcome the current limitations, significant research effort in the area of nanotechnology is focused on improving this quality of treatment through achieving an increase in the dose localisation to tumour sites, in addition to reducing non-specific systemic toxicity.

It is proposed that this can be achieved through promoting the selective accumulation of a carrier molecule specifically within tumour sites. It is well known that the vasculature surrounding a tumour is typically severely compromised as a result of the rapidly dividing nature of cancer cells, a phenomenon which has been exploited in nanomedicine through the Enhanced Permeation and Retention effect (EPR effect).[14] In addition to the leaky blood vessels, poor lymphatic drainage in the area contributes to enhanced retention of circulating particles.[15] This has led to the development of nanoparticle drug delivery carriers that can achieve preferential accumulation within tumour sites, and thereby have the ability to deliver drugs in more a targeted manner. This can additionally be improved upon

through the inclusion of specific targeting ligands, such as antibodies, peptides and small molecules that take advantage of specific antigenic interactions.[16] The addition of an active targeting ligand provides the drug delivery carrier with the capability for tumour cell uptake through the recognition of specific cell-surface receptors for surface binding.[17] This can translate into increased control over the final accumulation and biodistribution of the carrier following systemic injection. Both passively and actively targeted particles are likely to accumulate in the tumour site through the EPR effect, however, following localisation within the interstitial space, particles with an appropriate active targeting ligand will then recognise their receptor target, bind, and be retained within the tumour environment. Additionally, if the target receptor is internalising, this is then followed by internalisation into the cells.[18] This is an especially important consideration for drugs that act intracellularly, indicating that internalisation is mandatory for an efficient therapeutic effect, such as in gene delivery.

Utilising a biocompatible 'stealth' polymer carrier is an approach towards this that has been widely investigated.[19-22] The construction of biocompatible nanoparticles with a PEG coating for example, provides a carrier vehicle with long circulation times *in vivo* through both an increased size, and the ability to evade clearance from the bloodstream by the mononuclear phagocyte system (MPS).[23, 24] There exist many examples in the literature in which nanoparticles have demonstrated their versatility through functionalisation with various components for imaging, targeting and drug delivery, such as nanoparticles featuring active targeting ligands and encapsulating therapeutic drugs.[25, 26] A further advantage of utilising a polymer based system is that the circulation times and clearance mechanisms of the nanoparticles are able to be tuned through manipulation of the properties of the carrier material, for example to allow long-term sustained released through controlled erosion, or capsule degradation at the active site through the use of biodegradable monomers.[27-30]

The other important aspect that must be considered is how the drug will be incorporated into the nanoparticle. Several early examples of drug delivery nanoparticles feature the drug cargo encapsulated within a central cavity, such as within a liposome or a vesicle.[31] However, this method does not allow for precise control over the encapsulation and release of the drug, and physically encapsulated drugs can also be prone to leakage from the carrier while in circulation.[32-35] An alternative design is to tether the drug to the nanoparticle through a covalent linkage. While attachment of drugs to nanoparticle carriers through covalent chemistry requires more sophisticated synthetic requirements, the resultant system will typically be more stable to unwanted burst release of the drug, can facilitate a higher loading efficiency, and provides additional control over both the rate of the release and the site of drug release *in vivo*.[36-38] The release of the drug from the nanoparticle can be triggered through degradation of the covalent attachment, which can be achieved through a range of biological environments present in the target location. Typical *in vivo* conditions that are exploited for this purpose are the acidic environment of a tumour, the acidity of the endosome, and the enzymatic environment of the cell cytosol.[39-43] An actively-targeted nanoparticle will be localised within endosomes following endocytosis, which have pH ranges of ~4.5 to 6.5, providing opportunity for stimuli-responsive release through acid-labile linkages.[44] There are several covalent linkages that are commonly used for this purpose, including an acetal, ester or a hydrazone bond, which when used in conjunction with a targeted nanoparticle towards these environments will allow for specific release of the drug payload in the extracellular or vesicular sites.[45-47]

Our group has previously described a theranostic based on a hyperbranched polymer platform with targeting capabilities for prostate cancer through a small molecule ligand for Prostate Specific Membrane Antigen (PSMA).[48] PSMA has been identified as a specific cell-surface receptor that is overexpressed on many prostate cancers, as well as on lymph node and bone metastases of the disease, but with low levels detected on normal prostate tissues. Therefore, PSMA is considered a promising candidate for the specific delivery of nanoparticles to prostate cancer, with PSMA-targeted nanoparticles in clinical trials. Our previous work demonstrated preliminary evidence of stimuli-responsive drug delivery capabilities through the inclusion of a hydrazide monomer within the backbone of the hyperbranched polymer, which allowed for attachment of a model fluorescent drug through formation of hydrazone bonds. Here, we present further work on this system by exploring the targeted, stimuli-responsive controlled release of a chemotherapeutic through more extensive *in vitro* and *in vivo* characterisation, with efficacy of the nanomedicine as a therapeutic demonstrated in tumour regression studies in mice. The overall approach is described in Scheme 1.

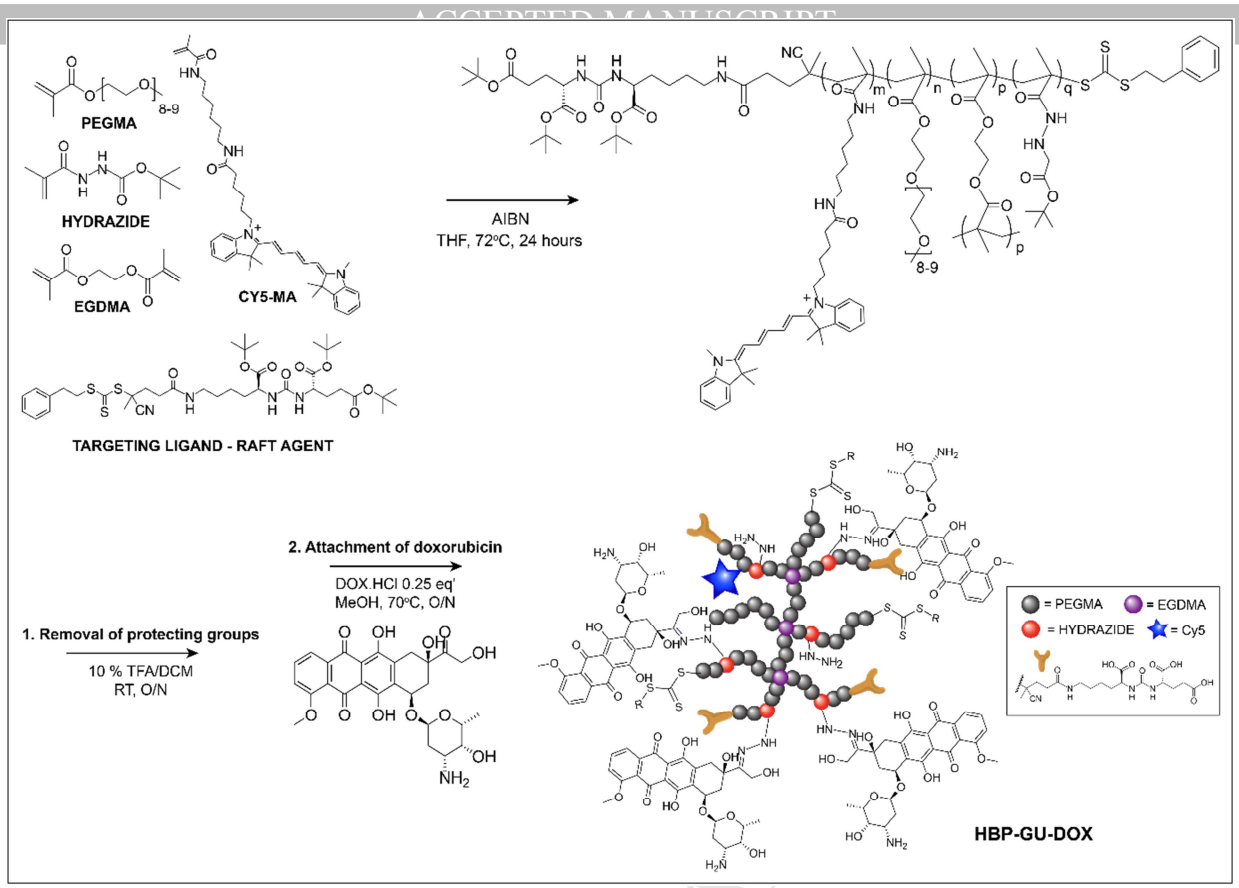

Scheme 1. The overall reaction scheme for the formation of HBP-GU-DOX. The base polymer carrier was synthesised by RAFT polymerisation, followed by attachment of doxorubicin through hydrazone formation.

Experimental

Characterisation Methods

All NMR experiments were undertaken on a Bruker Avance 500 high-resolution NMR spectrometer. ^{1}H NMR spectra were collected for 128 scans. All ^{1}H diffusion spectra were recorded at 500 MHz at 95% gradient, ambient temperature, and 256 scans.

In vitro flow cytometry was performed on an Accuri C6 Flow Cytometer (BD Bioscience, San Jose, CA) using the 640 nm laser collecting through the 675/25 filter (Cy5).

In vitro microscopy images were acquired on a Carl Zeiss LSM 710 confocal laser scanning microscope.

In vivo optical imaging experiments were performed on an In Vivo MS FX Pro instrument (now supplied by Bruker Corporation). Cy5 images were collected with a 630 ± 10 nm excitation and 700 nm ± 17.5 nm emission filter set (f- stop 2.80, 2 × 2 binning, 190 mm FOV, 10 sec exposure time). DsRed fluorescence images were collected with a 550 ± 10 nm excitation and 600 nm ± 17.5 nm emission filter set (f-stop 2.80, 2 × 2 binning, 120 mm FOV, 20 s exposure time). To provide anatomical context, fluorescence images were co-registered with an X-ray image (f-stop 2.80, 0.2 mm aluminium filter, 190 mm FOV, 30 sec acquisition time). All images were batch exported as 16-bit TIFF images and image processing was completed using Image-J (National Institutes of Health). Fluorescence images were false coloured and overlaid onto X-ray images.

Hyperbranched polymer synthesis

The hyperbranched polymers used in this study were synthesised as previously described.[48] For this study they were labelled HBP-GU (glutamate urea targeted) or HBP (untargeted control).

Doxorubicin attachment to hyperbranched polymer (HBP-GU-DOX)

HBP-GU (20 mg, 5.7 x 10^{-2} mmol) was dissolved in 100 µL dry methanol in a glass vial equipped with a stirrer bar. DOX.HCl (1.69 mg, 2.92 x 10^{-3} mmol, 0.25 eq' to hydrazides) was added and the reaction stirred overnight at 40 ^{o}C. The reaction was purified by precipitation into hexane/diethyl ether 3 times, followed by size exclusion purification using a

prep column in 20 % EtOH/H_20. DOX attachment was characterised by ^{1}H NMR, UV-Vis and fluorescence microscopy (ex = 480 nm, em = 580 nm).

***In vitro* buffer release study**

Phosphate buffer solutions at pH 5.5 and 7.4 were used to simulate endosomal and physiological pH. A calibration curve of DOX.HCl was prepared by measuring ten concentrations in a 48 well plate in pH 7.4 phosphate buffer. The excitation and emission wavelengths were 480 nm and 580 nm respectively. The samples were measured in a Tecan plate reader at a depth of 19 mm with 10 flashes and an integration time of 20 µs.

The following release study was performed in triplicate to account for statistical variation between subsets. 1.0 mg of HBP-GU-DOX was dissolved in 1 mL pH 7.4 phosphate buffer. The dissolved polymer was added into a 3.5 kDa MWC dialysis cassette, and placed into a sealed glass apparatus containing 100 mL of either pH 7.4 or 5.5 phosphate buffer. All samples were stirred at 37 ^oC for 48 hours. Aliquots of the dialysis buffer (1 mL) were removed at various time points, replacing with fresh buffer. The samples were measured on the plate reader using the same settings as the standards.

***In vitro* cell uptake study**

Studies were undertaken to analyse the uptake and stability of the HBP-DOX conjugates in cell growth medium. Human prostate cancer LNCaP cells were seeded into 24 well plates (4.0 x 10^4 cells per well) and incubated overnight with RPMI(Life Technologies, Mulgrave, Vic, Aust) containing 10 % foetal bovine serum (FBS; Moregate, Brisbane, Aust) at 37 ^oC with 5% CO_2. The incubation medium was removed and 500 µL of polymer-containing medium at various concentrations was added to each well. The cells were incubated at 37 ^oC for 30 mins, 2 hrs or 4 hrs. Following incubation the polymer solution was removed and the cells were washed with fresh RPMI three times. Cells were detached from the wells using trypsin-EDTA and transferred to Eppendorf tubes containing 1 drop of FBS. The cells were centrifuged into pellets, resuspended in PBS and analysed by flow cytometry.

***In vitro* cytotoxicity**

For cytotoxicity measurements, LNCaP prostate tumour cells were seeded into 96 well plates at a density of 1.5 x 10^3 cells per well in 100 µL of RPMI. The cells were allowed to adhere in growth media overnight at 37 ^oC. The cell media were discarded and replaced with fresh media (100 µL) containing either free doxorubicin, HBP-GU or HBP-GU-DOX at eight different concentrations, each in triplicate. The cells were incubated for either 24 or 48 hours; these incubation times were devised based on the release profile of the DOX from the hyperbranched polymers. Cell viability was then assessed by 3-(4,5-dimethylthiazol-2-yl)-5-(3-carboxymethoxyphenyl)-2-(4-sulfophenyl)-2H-tetrazolium (MTS) assay (CellTiter 96 AQuesous One Solution Cell Proliferation Assay; Promega) following provided manufacturers methods. Briefly, wells were washed once with 200 µL growth media before addition of 100 µL of growth media containing 20% (v/v) MTS assay reagent. Plates were incubated for 30 mins at 37 °C and absorbance at 490 nm of each well was measured. Absorbance readings of blank wells (no cells) were subtracted from all readings and then values were normalised to cells grown in the absence of test compounds. Cell viabilities were calculated and statistical significance calculated through unpaired t-tests (Significance $P<0.05$).

***In vitro* confocal microscopy**

Live cell confocal microscopy was performed on the HBP-GU, HBP-GU-DOX and free DOX to further quantify uptake into LNCaP tumour cells in real-time. In preparation for imaging, a suspension of LNCaP cells was plated into Ibidi^{tm} coverslip-bottom µ-dishes (0.5 mL per dish) supplemented with 2 mL of complete RPMI media, returned to the incubator and left overnight. Imaging of intracellular distribution and doxorubicin release was performed on a Zeiss 710 inverted laser scanning confocal microscope equipped with a 40x water immersion lens in addition to Argon and Helium-Neon lasers. Prior to imaging, cellular morphology and health was assessed using brightfield imaging. 40 µL of a 0.25 µM solution of HBP-GU or HBP-GU-DOX or 40 µL of a 1.21 µM free DOX was added to the media and the cells were monitored over time. Example cells were selected, the field of view and zoom factor altered and the resolution optimised using the inbuilt function in the Zeiss software. As the control polymer and DOX concentrations were matched to the targeted DOX loaded polymer, channel settings such as gain were determined from DOX and Polymer alone samples. Images were post-processed using Zen Lite 2012 (Blue Edition) (Carl Zeiss Microscopy GmbH), being smoothed with a Gaussian Filter (Sigma value of 0.9 in both the X & Y directions), prior to being exporteds as TIF files with no compression. Fluorescence intensity was extracted using the Zen Lite software from the raw data files using the Regions of Interest (ROI) tool to select cellular features and the measure capabilities for statistical analysis.

***In vivo* imaging**

All studies were in accordance with guidelines of the Animal Ethics Committee of The University of Queensland (UQ), and Australian Code for the Care and Use of Animals for Scientific Purposes. Studies were undertaken to quantify the *in vivo* behaviour of the doxorubicin-loaded glutamate urea-targeted polymer, HBP-GU-DOX. A male nu/nu mice was implanted subcutaneously with 2×10^6 PSMA positive PC3-PIP cells on the right flank. The imaging experiment was performed 11 days after tumour cell injection. HBP-GU-DOX was diluted in PBS to 5 mg mL^{-1}, and 200 µL was injected into the mouse via the tail vein. Fluorescence and XRay images were acquired using an In Vivo MS FX Pro imaging station. Mice were anaesthetised with 2 % isoflurane during all procedures.

***In vivo* tumour regression study**

13 male nu/nu mice were injected with LNCaP cells in the left flank to induce subcutaneous tumours. The mice were split into 5 groups, 3 x control (saline), 2 x control (HBP-GU), 3 x free DOX, 2 x HBP-DOX and 3 x HBP-GU-DOX. HBP-GU-DOX, HBP-DOX and free DOX was administered at a DOX concentration of 4.5 mg/kg, with the control polymer equal to the HBP-GU-DOX polymer concentration. After the tumours reached approximately 75 mm^2 in volume (tumour volume = ½ (*length* × *width* ^{2}))[49], the mice received the appropriate treatment intravenously on days 1, 3, 7, 11 and 18, except for the HBP-DOX group which was dosed on day 14 instead of day 11.[50] The mice were monitored, including body mass and tumour volume measurements over a 28 day period. At the end of the 28 day period, or once tumours reach 1000 mm^3 in size, the mice were culled and their organs and tumour removed and imaged in an MSFX Pro to visualise polymer accumulation within the tissues (ESI, Figure S4).

Results and Discussion

Drug attachment and characterisation

The aim of this work was to investigate the efficacy of a doxorubicin-loaded hyperbranched polymer targeted to prostate cancer, through the use of a small molecule glutamate urea as previously described by our group.[48] Doxorubicin was chosen as the chemotherapeutic for this study, as it is a well-documented anti-cancer agent that is effective on some prostate cancer cells, and furthermore it has the ability to act as a fluorophore, enabling efficient characterisation *in vitro*.[51, 52] Additionally, doxorubicin inherently features a sterically-unhindered ketone functionality suitable for hydrazone formation with a hydrazide, enabling it to be used in this study without further modification.[53, 54]

Refluxing the hyperbranched polymers featuring hydrazide moieties in methanol overnight with DOX.HCl (0.25 equivalents of DOX to hydrazides) resulted in a high percentage of functionalisation (94 %). This demonstrates close to quantitative attachment of DOX to the hydrazides within the polymer backbone, and therefore that the hyperbranched system can successfully facilitate drug loading in high yield. As the DOX-loaded polymers were to be utilised for imaging studies, the DOX was reacted at 0.25 equivalents to hydrazide in order to ensure the final polymers had approximately equal emissions of both DOX and Cy5. Following the hydrazone formation with the DOX, the HBP was purified through size exclusion to ensure no free DOX remained in the system. The DOX concentration per polymer was subsequently characterised by quantitative ^{1}H NMR (the representative peaks b,c,d,h are highlighted in Figure 1), which allowed the calculation of an average of 1.1 DOX molecules per arm of the hyperbranched polymer. By utilising SEC with multiangle laser light scattering (MALLS) to quantify the absolute molecular weight of the polymers, the total number of arms within each hyperbranched polymer was calculated to be an average of 4.6, and therefore the total number of DOX molecules per hyperbranched polymer was calculated to be 5.06. This was confirmed through UV-Vis spectroscopy (480 nm), utilising a standard curve of free DOX, which calculated a total of 4.62 DOX per polymer. The total number of DOX molecules per polymer was taken as an average of both techniques: 4.84 DOX molecules per HBP. The diameter of the hyperbranched polymers was measured by DLS, and found to be 6.2 nm.

Table 1. Summary of the physical and chemical properties of the final DOX-loaded and PSMA-targeted hyperbranched polymer (HBP-GU-DOX)

Mn (^{1}H NMR)	Mn ($Đ_M$) SEC-MALLS	# hydrazides / polymer	Theoretical # DOX*	# DOX (^{1}H NMR)	# DOX (UV-Vis)	D_h^
8.5 kDa	39 kDa (1.7)	20.42	5.11	5.06	4.62	6.2nm

* Theoretical DOX calculated based on feed ratio and 100 % coupling efficiency. ^Size measurement calculated from HBP-GU.

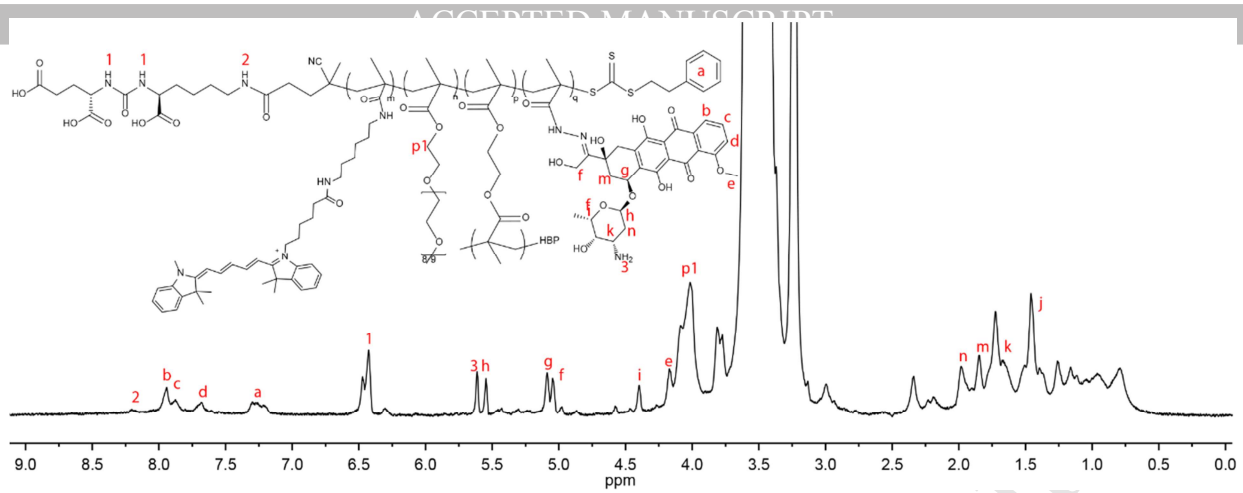

Figure 1. ^{1}H 1D DOSY NMR spectra of the HBP-GU-DOX confirming the successful hydrazone formation with the drug. Resonances used for quantification of DOX attachment are highlighted (b, c, d and h).

***In vitro* characterisation of the polymer-drug conjugate**

Following the attachment, purification and characterisation of the DOX loading onto the hyperbranched polymers, an initial *in vitro* buffer release experiment was conducted to determine the stability of the conjugates, as well as their release kinetics under physiologically relevant conditions of pH. The HBP-GU- DOX was dialysed in either pH 5.5 (endosome conditions) or7.4 (serum conditions) phosphate buffer at 37 ^{o}C for 48 hours, during which time the buffer was measured at various time points for the DOX concentration, which is indicative of release from the polymer system. Utilising standards of free DOX, the data was able to be transformed to represent the percentage release of the initial total DOX from the HBPs over time. As previously shown by many researchers, the DOX-conjugated polymer demonstrated remarkable stability at neutral pH, with less than 10 % release at pH 7.4 over 48 hours.[46, 55] However, during this same timeframe at an acidic pH of 5.5, such as in the endosome, 90 % of the initial conjugated DOX was able to be released in a controlled manner, with no burst release, and a half-life of 12 hours (Figure 2A). This experiment therefore provided preliminary confirmation of the viability of the HBPs for controlled, stimuli-responsive drug delivery.

Following the initial release experiments, the next investigation probed the reproducibility of the *in vitro* release kinetics in a cellular environment. This was done through both *in vitro* uptake studies of the HBPs into LNCaP prostate cancer cells, as well as *in vitro* cytotoxicity assays over extended time points. Initially, both DOX-loaded and unloaded glutamate urea targeted HBPs were incubated with LNCaP prostate cancer cells and their uptake quantified using flow cytometry. HBP-GU-DOX, HBP-GU and an additional control untargeted polymer (HBP) were used at concentrations ranging between 0.025 µM to 0.2 µM, over three time points: 30 mins, 2 hours and 4 hours. After incubation with the polymer solutions, the cells were washed and resuspended in PBS for flow cytometry analysis. The ability of the glutamate urea targeted polymers to selectively bind to PSMA+ cells was confirmed, with a clear trend of increasing Cy5 signal, and thus polymer uptake, into the LNCaP cells with increasing concentration and incubation time. As a control, untargeted HBP was also tested, and demonstrated significantly lower uptake into the LNCaP cells, confirming that uptake is likely due to the inclusion of the active targeting ligand. Importantly, the HBP-GU-DOX did not behave significantly differently to the HBP-GU, suggesting that there is no detrimental effect on polymer uptake with the inclusion of the hydrophobic drug (Figure 2B). Analysis of the percentage of cells that were alive during the flow cytometry experiment did not show a significant cytotoxic effect on the cells over the short time frame tested, which is consistent with the timeframe of DOX release as described by the buffer release study (Figure S3, ESI).

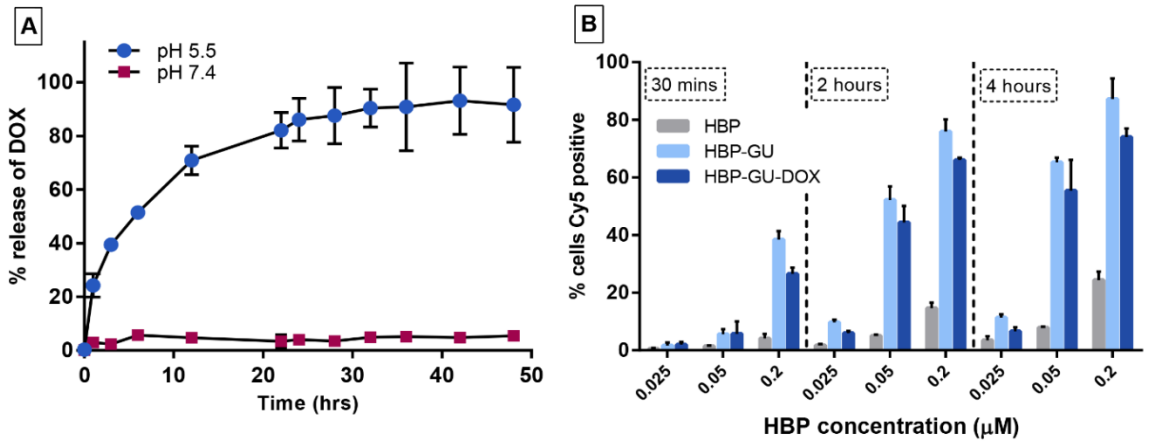

Figure 2. Data showing A) the in vitro buffer release profile of DOX in simulated in vivo conditions, and B) uptake of the HBPs in LNCaP prostate cancer cells demonstrating increased uptake over concentration and time when an active targeting ligand is featured on the surface of the nanoparticle. Data represents mean ± SD (n = 3).

Following the confirmation of selective uptake into the tumour cells by the glutamate urea targeting ligand, cytotoxicity studies were completed to quantify the toxicity of both the unloaded HBP-GU and the DOX-loaded HBP-GU in comparison to free DOX. If the DOX is able to be released in the endosome through hydrolysis of the hydrazone bond following internalisation, the resultant free DOX should then be able to impart toxicity on the cell, triggering apoptosis. Therefore, if the HBP is successful in delivering DOX to the endosome within the cells, we hypothesised that the cytotoxicity should be similar to that of free DOX beyond the timeframe of DOX release. In order to quantify this, LNCaP cells were incubated with their respective treatment at eight different concentrations over both 24 and 48 hours. The cell viability was analysed through an MTS assay, with untreated cells utilised as a baseline reading for cell viability over the experiment. The cytotoxicity of each polymer sample was quantified as a percentage of viable cells from a ratio of the untreated cells.

As expected, over the initial 24 hour period, both the HBP-DOX and free DOX were able to reduce cell viability to 65 % and 45 % respectively for the highest concentrations of DOX, suggesting that the DOX was successfully released from the polymer carrier and able to induce apoptosis within the cell (Figure 3A). This conclusion was supported by the control HBP demonstrating no toxicity over the same concentration range and time frame (90 % cell viability for the highest concentration). This result is consistent with the buffer release study, where at 24 hours almost 80 % of the DOX had been released from the HBP-GU-DOX. By 48 hours, the control HBP remains nontoxic to the cells, with 90 % cell viability at the highest concentrations of polymer, while the cytotoxic effect from the DOX is increased in both the HBP-DOX and free DOX samples (Figure 3B) to 30 % and 20 % cell viability respectively at the highest concentrations of DOX. This is likely due to a combination of further release of the DOX from the HBP through continued hydrolysis of the hydrazone bond, in addition to the prolonged exposure of the cells to the DOX during the additional 24 hour period.

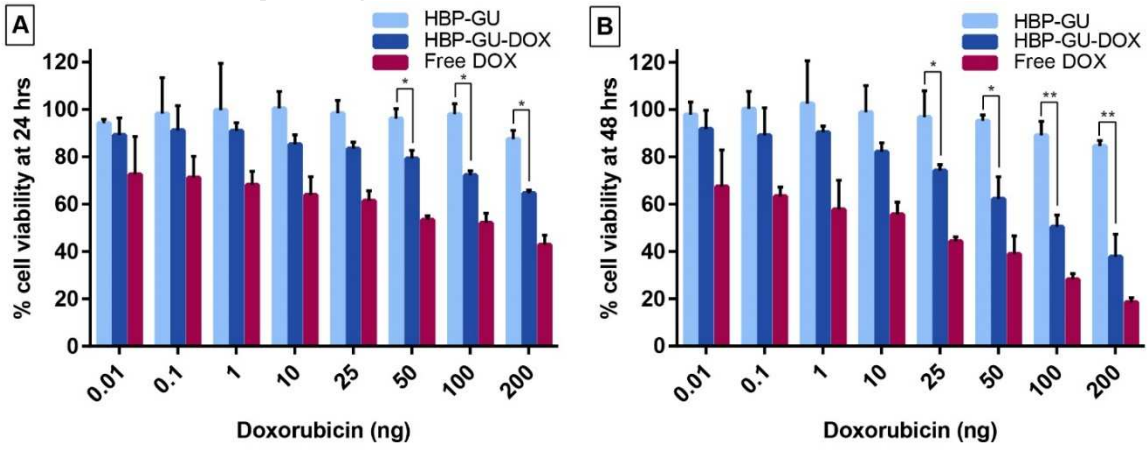

Figure 3. The cytotoxicity of the HBP, free DOX and the HBP-DOX conjugate on LNCaP tumour cells at A) 24 hours and B) 48 hours as quantified by an MTS assay. Data represents mean ± SD (n = 3), statistical significance calculated through unpaired t-tests (Significance P<0.05).

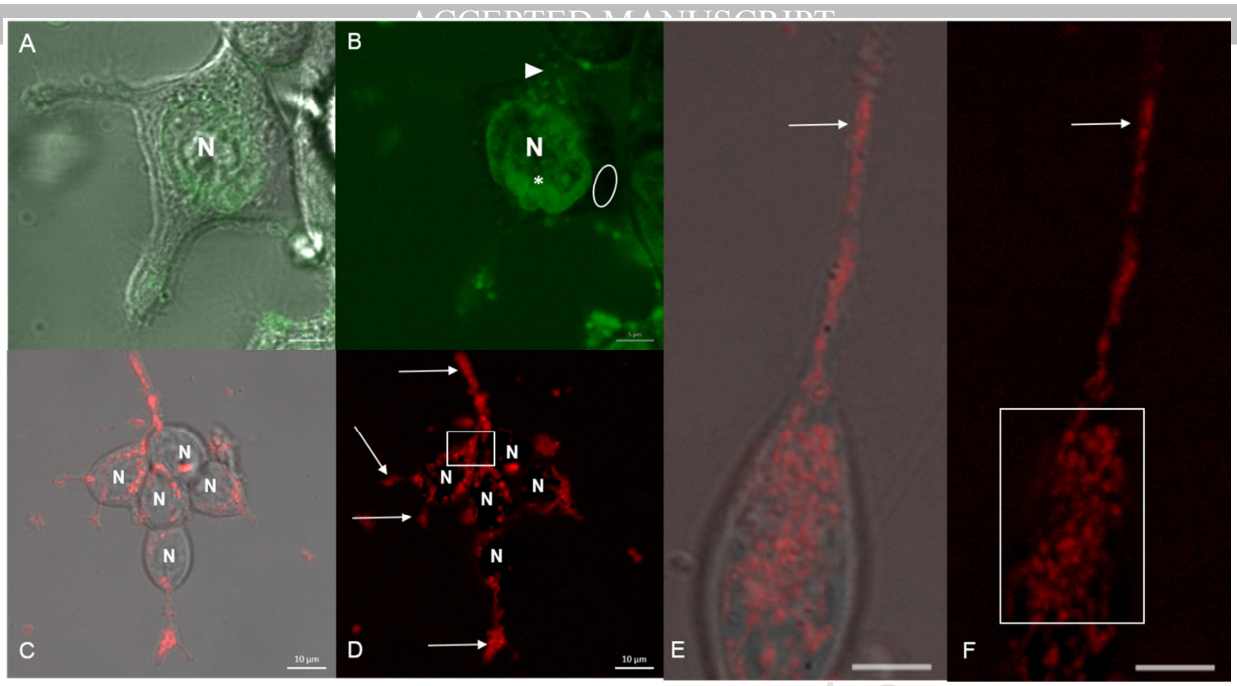

Figure 4. Confocal micrographs of DOX and HBP-GU distributions in live LNcaP prostate cancer cells at 2 hours post exposure. A) DOX staining with brightfield overlay, features indicated in the fluorescence only image of the same cell, B) include nuclear staining (asterisk), diffuse cytoplasmic staining (arrowhead) and an example of a region with much lower than background fluorescence in the cellular milieu (oval). Examples of cells showing uptake of GU-HBP are given in (C & D), a brightfield overlay being presented in C). Features labelled by the material include focal adhesions (arrows) and a combination of vesicular and filamentous structures (an example is highlighted by a rectangle). Higher magnification image from towards the basal surface of an example cell displaying these features is given with a brightfield overlay e) and Cy5 fluorescence alone F) illustrating vesicular structures (rectangle) and focal adhesion staining (arrows) in greater detail (scale bar in E & F is 5 µm). Where applicable, nuclei are marked (N).

The ability for the hyperbranched polymers to deliver the DOX into the cells through receptor-mediated internalisation was further characterised through live cell confocal microscopy. The rationale behind this experiment was to analyse the mechanism of DOX internalisation into cells when the DOX was tethered to a polymer carrier, as compared to free DOX in solution. In order to investigate this, the internalisation of HBP-GU-DOX, free DOX and HBP-GU as a polymer control were qualitatively analysed in live LNCaP cells. Immediately prior to imaging, the respective treatment (diluted in cell culture media) was added on top of the cell monolayer, after which images were acquired at regular time points utilising the appropriate emission filters. The internalisation behaviour and cellular distribution of the control HBP-GU and the free DOX were used as the expected baseline behaviour for the internalisation of a polymer and small molecule chemotherapeutic respectively, for the comparison of the behaviour of the polymer DOX conjugate.

The HBP-GU and free DOX indeed demonstrated different behaviours *in vitro.* Figure 4 shows representative live cell confocal micrographs taken at 2 hours post exposure to the respective treatment. It can be seen in Figure 4 (A & B) that the DOX was successfully able to travel into the LNCaP cells over time. However, the images suggest that the DOX relied on passive mechanisms of diffusion into the cells, which resulted in diffuse cytoplasmic staining. In comparison, Figure 4 (C–F) demonstrates that the HBP-GU was also successfully able to transport into the cells, however, the polymer displays more sophisticated methods of internalisation, suggesting receptor-mediated transport. This is illustrated by trafficking along the focal adhesion and the combination of punctate and filamentous staining within the cellular milieu, which is indicative of vesicular transport. Furthermore, it can be seen that after 2 hours, the localisation of fluorescent signal within the cells is different for the DOX and HBP-GU. After 2 hours, the free DOX shows significant fluorescence within the cell nuclei. This is expected behaviour, as the mechanism of action for DOX is to bind to DNA, and therefore, following passive diffusion into the cell cytoplasm, the DOX was clearly able to accumulate within the nucleus. This was not observed for the HBP-GU; after 2 hours, the polymer is still retained within vesicles in the cells, as demonstrated by specific vesicular staining within the cytoplasm, further supporting receptor-mediated endocytosis as the route of cell internalisation.

The images acquired of the HBP-GU-DOX *in vitro* demonstrate behaviour that is consistent with that of the control HBP-GU (Error! Reference source not found.). It can be seen that the staining and localisation of the Cy5 fluorescence within the cells is comparable to that of the HBP-GU, confirming that the HBP-GU-DOX is also able to transport into the cells through receptor- mediated internalisation. Of particular note, the staining of DOX within the

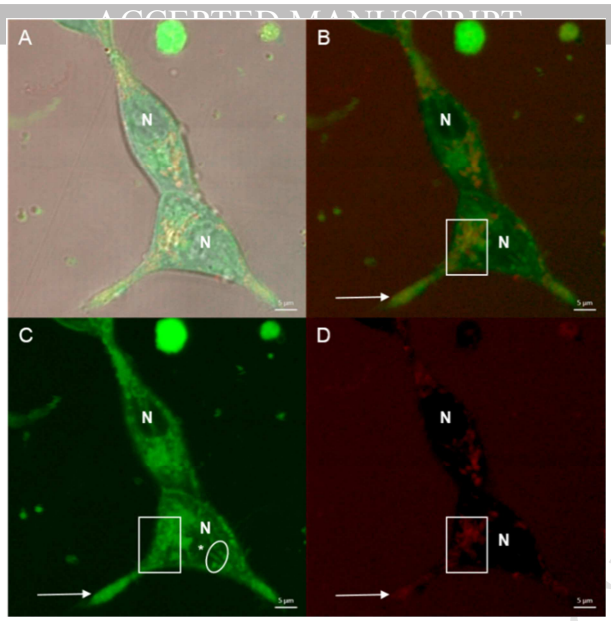

Figure 5. Confocal micrographs of HBP-GU-DOX in live LNcaP prostate cancer cells at 2 hours post exposure. A) dual-coloured image with brightfield overlay, B) combined doxorubicin and Cy5 fluorescence, C) doxorubicin channel, D) Cy5 channel. Focal adhesion staining is labelled with an arrow, vesicular structures a rectangle, filamentous features with an oval and nuclear fluorescence is indicated (asterisk). Nuclei are marked (N).

cells displays significantly different behaviour in these images. Rather than diffuse cytoplasmic staining, the DOX is showing obvious staining of the focal adhesions and highlighting vesicular and filamentous structures in the cellular milieu, mimicking the staining patterns for the HBP-GU, and thus confirming the ability of the polymers to facilitate specific DOX transport into the cells. In addition to the vesicular localisation of the DOX within the cells, by 2 hours post exposure, the DOX is beginning to demonstrate some characteristic nuclear staining. From the buffer release study, in simulated endosomal conditions, the HBP-GU-DOX demonstrated slow and controlled release of the DOX from the polymers over approximately a 30 hour period, with approximately 30 % released over the first 120 minutes. It is thus expected to see the DOX remaining bound to the polymer initially within the cells, as seen in the localisation of the DOX within vesicles, with evidence of some release by the 2 hour images. Thus, these images support the hypothesis that following internalisation into the endosome, the DOX is able to be released from the polymer carrier through hydrolysis of the hydrazone linkage, exit the endosome and travel into the nucleus.

In order to further understand the different behaviours of each sample within the cells, and to confirm the qualitative analysis based on the confocal images, the localisation of the fluorescent signal within the cells was analysed quantitatively through ROI analysis (Figure 6). In the same 2 hour images, regions of interest were drawn within various compartments within the cells and normalised to the maximum fluorescence intensity found within the entire image. The ROI analysis was able to quantitatively confirm the difference in intracellular localisation between the free DOX and the DOX-loaded HBP.

For free DOX, significant signal is located within the nucleus after 2 hours, with minimal localisation within the cytoplasm and vesicles. However, the DOX signal for the HBP-GU-DOX demonstrates predominant localisation within vesicles and the cytoplasm, with significantly less fluorescence located within the nucleus. The Cy5 fluorescence does not appear to vary significantly between the DOX-loaded and unloaded polymers, confirming that the inclusion of the DOX within the polymers does not have a significant effect on the method of transport into the cells. Additionally, the ROI analysis confirms that the predominant source of Cy5 fluorescence is within vesicles, focal adhesions and the cytoplasm, with negligible signal in the nucleus. However, by the 2 hour images, the HBP-GU-DOX shows higher DOX signal in the nucleus than Cy5 signal, which supports the hypothesis of DOX release following internalisation and localisation within vesicles, triggering degradation of the hydrazone linkages. All of this information taken together suggests that the targeted polymer enhances rapid accumulation of the nanomedicine within the cell through receptor-mediated endocytosis, with subsequent release of the DOX which then migrates to the nucleus of the cell.

***In vivo* tumour regression study of polymer-drug conjugate**

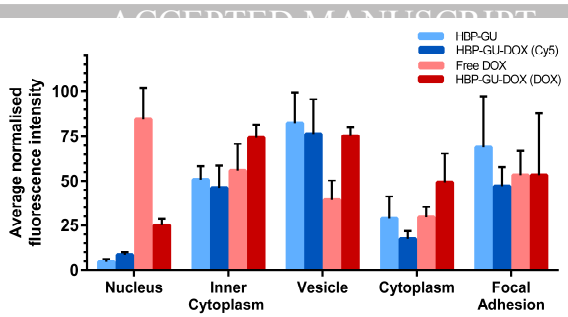

Figure 6. The average fluorescence intensity within various cellular compartments based on ROI analysis of the confocal micrographs at 2 hours post exposure. Data represents mean ± SD (n = 4).

The extensive *in vitro* characterisation described above confirms the selective and stimuli-responsive delivery of doxorubicin to PSMA-positive cells through the glutamate urea targeted HBPs. Following this, the ability for the HBP to impart a therapeutic effect on tumour cells in animal models was investigated. The intent behind developing targeted, nanoparticle drug delivery carriers is in the specificity and increased efficiency of treatment; it is desired that the nanoparticles are able to deliver a therapeutically effective dose to the tumour site with minimal non-specific toxicity elsewhere in the body.

Prior to conducting an *in vivo* tumour regression study to assess the suitability of the HBP-GU-DOX for this purpose, an *in vivo* imaging study was performed in order to confirm that the *in vivo* behaviour of the targeted DOX-loaded polymer was not significantly affected by the presence of the hydrophobic drug within the polymer core. It was hypothesised that there would be no significant effect due to both the relatively low incorporation of the drug within the polymer (6% w/w), and the branched, hydrophillic nature of the HBPs. To compare with previous *in vivo* studies of the polymer without drug, a male nude mouse was implanted with a subcutaneous PC3-PIP (PSMA-expressing) tumour. The tumour was allowed to grow for 11 days, and then HBP-GU-DOX was injected via the tail vein and fluorescence images acquired at 24 hours post-injection. The resultant images (Figure 7) confirm behaviour comparable to that of the unloaded HBP-GU as in previous work.[48] By 24 hours there is significant accumulation of the polymer within the subcutaneous tumour, as well as signal in the region of the kidneys, indicating clearance through this route. The size cut-off for renal clearance is approximately 6 nm, and therefore it would not be expected to see clearance through this route if any significant micellisation or aggregation were occurring.[56, 57] Any materials that are larger than 8 nm, and therefore unable to filter through the kidneys, are expected to be cleared through hepatic routes. There is no polymer signal in the region of the liver, and therefore it can be concluded that the drug-loaded polymers are stable *in vivo*.[56]

Following confirmation of the consistent *in* vivo behaviour between drug-loaded and non-loaded polymers, the ability of the HBP-GU-DOX to impart a therapeutic effect was investigated through a tumour regression study. 13 nude mice had subcutaneous LNCaP tumours induced on the left flank. After the tumours had grown over a 6 week period, the mice were divided into five treatment groups: saline control, HBP-GU control, HBP-DOX, HBP-GU-DOX and free DOX. The mice received intravenous injections of the relevant treatment on pre-determined days over a 28 day period (Figure 8). Throughout the 28 days, the health of each mouse was monitored through their body mass, and the size of the tumour measured through calliper measurements. The tumour volumes were calculated using a standard volume formula as previously reported (tumour volume = ½ (*length* × *width* ^{2}). At the end of the 28 days, or once tumour volumes reached over 1000cm^3, the mice were culled and the tumours measured *ex vivo* to confirm the accuracy of the *in vivo* measurements. The resultant data was transformed into a percentage of the original body mass and tumour volume for comparison between the five experimental groups. It can be seen in Figure 8B that as expected, the tumours in the saline control group continued to grow substantially over the experimental period. Likewise, the control polymer group, HBP-GU, did not have a therapeutic effect on the subcutaneous tumours, with the tumours from both control groups growing to approximately 300 % of their original volume. The untargeted HBP-DOX was also unsuccessful at inducing a therapeutic effect in the animals; while the growth of the tumours was not as significant as in the two control groups, perhaps indicating some arrest of tumour growth, by the end of the study the tumours were at 200 % of their original volume.

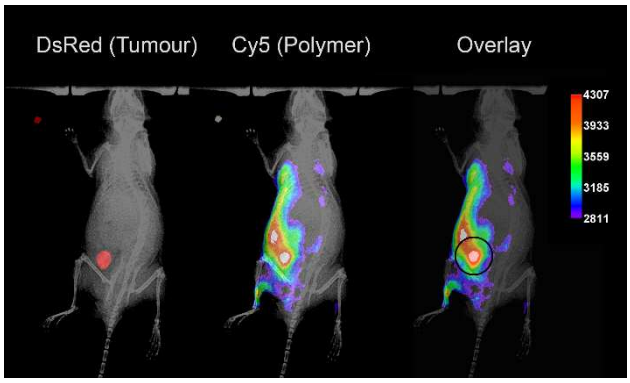

Figure 7. Nu/nu mouse with subcutaneous PSMA-expressing tumour on right flank. Fluorescence images were taken 24 hours post injection with HBP-GU-DOX showing the location of the tumour (DsRed), the polymer (Cy5) and an overlay of the two signals demonstrating co-localisation of the targeted polymer with the PSMA-expressing tumour (black circle).

It can be seen that the control polymer was not toxic to the animals, as their body mass did not vary significantly over time. This was the expected result, as the *in vitro* cytotoxicity suggested that the control polymer was not toxic to the LNCaP cells, and PEG is well known to be biocompatible.[19, 22] The body mass of the animals in the saline control group and HBP-DOX group only suffered slightly, with the animals finishing at 92 - 93 % off their original mass at the end of the study, which is likely due to the larger tumours in these two treatment groups in comparison to the other three groups. The free DOX however, appeared to have an adverse effect on the health of the animals over the 28 day period and imparted significant toxicity, with their body mass dropping rapidly by the end of the study by 20 % of their original mass. This was also the expected result, as it is well known that the toxicity imparted on other healthy cells in the body is a major disadvantage of systemically delivered chemotherapeutics.[58, 59] However, despite the significant toxicity to the animals, the DOX was able to partially arrest the tumour growth compared with the HBP control treatment, with the tumour volume decreasing by 30 % over the 28 days. This result is commensurate with similar studies in the literature, where the free drug was able to have an effect on tumour growth, but to the detriment of the overall health of the animals.[50, 60-62] Additionally, this result aligns with the live cell confocal microscopy results, which shed light on the mechanism of uptake of free DOX into the LNCaP tumour cells. The free drug relied on passive mechanisms of transport into the cells, and therefore due to the short circulation times that small molecules have

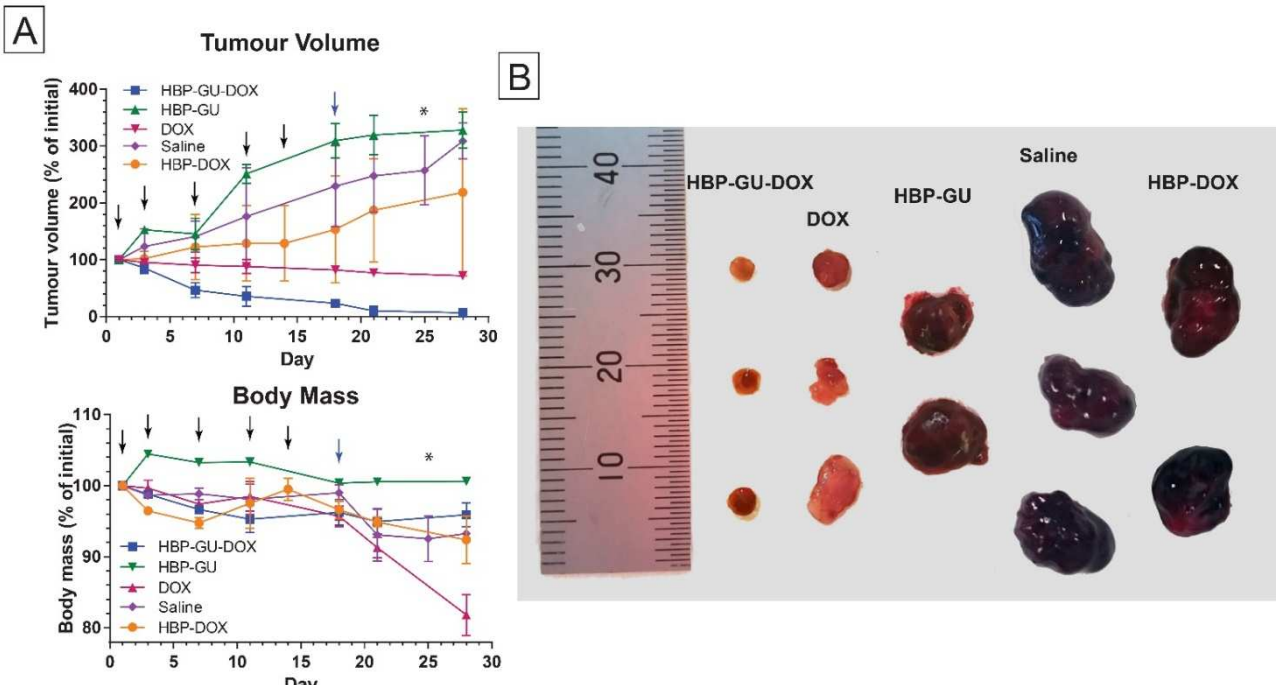

Figure 8. A) The tumour volumes and body mass of mice expressed as a percentage of the initial value, following a tumour regression study over 28 days and B) the excised tumours after the 28 day period. Arrows represent days on which mice were dosed (100 µL of 4.5 mg/kg in DOX), blue arrow represents treatment group dosed on day 14. Asterisk represents saline control mouse that was culled on day 25 for ethical reasons. Data represents mean ± SD (n = 2-3 mice).

within the body, it is likely that the DOX was cleared from the bloodstream too rapidly following intravenous injection to efficiently be accumulating within the tumour mass.[63] Importantly, the HBP-GU-DOX was indeed successful in imparting a therapeutic effect on the tumours *in vivo*. As seen in Figure 8A, the body mass of the mice did not vary significantly over the experiment, suggesting that the polymer did not lead to significant DOX release during circulation, and therefore not imparting non-specific toxicity on the animals. Additionally, the volume of the tumours decreased by over 90 % of their original volume over the 28 day period, confirming the ability of the hyperbranched polymer system to be successful as a targeted drug delivery carrier. Furthermore, following the final dose at 18 days, the tumours do not regrow, but rather continued decreasing in size out to the 28 day time point of the study. This overall result is in agreement with the live cell confocal microscopy, which confirmed that the HBP-GU-DOX was able to transport the DOX within the cells into vesicles, with significant accumulation and initial DOX release after 2 hours of exposure. As PEG-based polymers are known to have long circulation times *in vivo*, through a combination of the EPR effect and active targeting it is expected that significant accumulation of the HBP-GU-DOX within the tumour cells will occur. Evidently, following uptake into the cells through receptor-mediated internalisation into endosomes, the acidic environment was able to facilitate degradation of the hydrazone bond, and subsequent release of the DOX into the cell. It is important to note that this effect was only able to be observed with a combination of active targeting and drug loading, as seen by the lack of therapeutic effect from the HBP-DOX.

Conclusions

In this report we have demonstrated the successful synthesis of hyperbranched polymers with capabilities for targeted drug delivery to prostate cancer cells. The HBP system was able to facilitate a high loading efficiency (~90 %) of the chemotherapeutic doxorubicin through facile chemistry with hydrazide monomer units in the polymer backbone. The HBPs also featured a glutamate urea targeting ligand for PSMA-expressing prostate cancer cells, and an optical dye for *in vitro* and *in vivo* analysis. Characterisation through *in vitro* cell assays and live cell confocal microscopy demonstrated the ability of the DOX-loaded polymers to selectively accumulate within endosomes in PSMA-expressing LNCaP cells following receptor-mediated internalisation. Once inside the endosomes, the DOX-loaded polymers were shown to release the drug to induce a toxic effect, with DOX-loaded polymers demonstrating toxicity similar to that of free DOX over a 48 hour period. In comparison, no toxicity was observed in cells receiving the control HBP.

In order to demonstrate the ability of the HBP system to act as a theranostic, the therapeutic effect of the DOX-loaded polymers was assessed through a 28 day tumour regression study in mice. The mice received 5 intravenous injections of the HBP-GU-DOX over the 28 days, and demonstrated a ~90 % reduction in tumour volume over that time, with no significant change in their body mass. In comparison, free DOX only reduced the tumour volume by ~30 %, and caused significant toxicity to the mice, with 20 % loss of body mass over the course of the experiment. The controls of saline, HBP-GU and untargeted HBP-DOX did not show any therapeutic effect, with the tumour volumes considerably increasing over the time period. Importantly, the body mass of the mice did not decrease significantly, demonstrating the biocompatibility of the system *in vivo*. The hyperbranched polymer system demonstrated here therefore shows promise in a preclinical model as a theranostic for treating prostate cancer, and should be further explored in more clinically relevant models.

Acknowledgements

The researchers would like to thank Dr Christopher Howard (Australian Institute for Bioengineering and Nanotechnology, Australia) for the LNCaP cells used in this study. This work was performed in part at the Queensland node of the Australian National Fabrication Facility, a company established under the National Collaborative Research Infrastructure Strategy to provide nano- and micro-fabrication facilities for Australia's researchers. We acknowledge funding from the National Health and Medical Research Council (APP1046831, PJR, KJT, AKW), the Australian Research Council (FT110100284 (KJT), DP140100951 (KJT), DP110104299 (AKW)), and the Australian Commonwealth Government Australian Postgraduate Award (AKP). PJR was also funded in part by the Department of Health, Australia. This research was conducted and funded by the ARC Centre of Excellence in Convergent Bio-Nano Science and Technology (CE140100036).

References

1. D. M. Parkin, F. Bray, J. Ferlay and P. Pisani, *CA. Cancer J. Clin.*, 2005, **55**, 74-108.
2. M. C. Tsourlakis, F. Klein, M. Kluth, A. Quaas, M. Graefen, A. Haese, R. Simon, G. Sauter, T. Schlomm and S. Minner, *Appl. Immunohistochem. Mol. Morphol.*, 2015, **23**, 449-455.
3. S. K. Pal, P. Twardowski and O. Sartor, *Clin. Interv. Aging*, 2010, **5**, 395-402.
4. J. Ferlay, P. Autier, M. Boniol, M. Heanue, M. Colombet and P. Boyle, *Ann Oncol*, 2007, **18**, 581-592.
5. V. Kundra, P. M. Silverman, S. F. Matin and H. Choi, *Am J Roentgenol*, 2007, **189**, 830-844.
6. E. D. Crawford, M. A. Eisenberger, D. G. McLeod, J. T. Spaulding, R. Benson, F. A. Dorr, B. A. Blumenstein, M. A. Davis and P. J. Goodman, *New Engl. J. Med.*, 1989, **321**, 419-424.
7. M. A. Eisenberger, B. A. Blumenstein, E. D. Crawford, G. Miller, D. G. McLeod, P. J. Loehrer, G. Wilding, K. Sears, D. J. Culkin, I. M. Thompson, Jr., A. J. Bueschen and B. A. Lowe, *New Engl. J. Med.*, 1998, **339**, 1036-1042.
8. D. P. Petrylak, C. M. Tangen, M. H. Hussain, P. N. Lara, Jr., J. A. Jones, M. E. Taplin, P. A. Burch, D. Berry, C. Moinpour, M. Kohli, M. C. Benson, E. J. Small, D. Raghavan and E. D. Crawford, *New Engl. J. Med.*, 2004, **351**, 1513-1520.
9. A. Heidenreich, J. Bellmunt, M. Bolla, S. Joniau, M. Mason, V. Matveev, N. Mottet, H.-P. Schmid, T. van der Kwast and T. Wiegel, *Eur. Urol.*, 2011, **59**, 61-71.
10. K. Fizazi, C. N. Sternberg, J. M. Fitzpatrick, R. W. Watson and M. Tabesh, *BJU Int.*, 2010, **105**, 748-767.
11. I. V. Larina, B. M. Evers, T. V. Ashitkov, C. Bartels, K. V. Larin and R. O. Esenaliev, *Technol. Cancer Res. Treat.*, 2005, **4**, 217-226.
12. R. K. Jain, *J. Natl. Cancer Inst.*, 1989, **81**, 570-576.
13. J. H. Wasson, C. C. Cushman, R. C. Bruskewitz, B. Littenberg, A. G. Mulley, Jr. and J. E. Wennberg, *Arch. Fam. Med.*, 1993, **2**, 487-493.
14. A. Jones and A. L. Harris, *Cancer J. Sci. Am.*, 1998, **4**, 209-217.
15. K. Greish, *J. Drug Target.*, 2007, **15**, 457-464.
16. F. Marcucci and F. Lefoulon, *Drug Discov. Today*, 2004, **9**, 219-228.
17. J. D. Byrne, T. Betancourt and L. Brannon-Peppas, *Adv Drug Deliv Rev*, 2008, **60**, 1615-1626.
18. M. C. Garnett and P. Kallinteri, *Occup. Med.*, 2006, **56**, 307-311.
19. A. Vonarbourg, C. Passirani, P. Saulnier and J.-P. Benoit, *Biomaterials*, 2006, **27**, 4356-4373.
20. C. Lemarchand, R. Gref and P. Couvreur, *Eur. J. Pharm. Biopharm.*, 2004, **58**, 327-341.
21. C. Lemarchand, R. Gref, C. Passirani, E. Garcion, B. Petri, R. Müller, D. Costantini and P. Couvreur, *Biomaterials*, 2006, **27**, 108-118.
22. S. Kommareddy, S. B. Tiwari and M. M. Amiji, *Technol. Cancer Res. Treat.*, 2005, **4**, 615-625.
23. S. Stolnik, L. Illum and S. S. Davis, *Adv. Drug. Deliv. Rev.*, 2012, **64, Supplement**, 290-301.
24. M. Wang and M. Thanou, *Pharmacol. Res.*, 2010, **62**, 90-99.
25. A. Z. Abbasi, P. Prasad, P. Cai, C. He, W. D. Foltz, M. A. Amini, C. R. Gordijo, A. M. Rauth and X. Y. Wu, *J. Control. Release*, 2015, **209**, 186-196.
26. P. Chytil, E. Koziolova, O. Janouskova, L. Kostka, K. Ulbrich and T. Etrych, *Macromol. Biosci.*, 2015, **15**, 839-850.
27. J. Matsumoto, Y. Nakada, K. Sakurai, T. Nakamura and Y. Takahashi, *Int. J. Pharm.*, 1999, **185**, 93-101.
28. Y. Chen, V. J. Mohanraj and J. E. Parkin, *Lett Pept Sci*, 2003, **10**, 621-629.
29. A. Kumari, S. K. Yadav and S. C. Yadav, *Colloids Surf., B*, 2010, **75**, 1-18.
30. J. Panyam and V. Labhasetwar, *Adv Drug Deliv Rev*, 2003, **55**, 329-347.
31. C. Pinto Reis, R. J. Neufeld, A. J. Ribeiro and F. Veiga, *Nanomed. Nanotech. Biol. Med.*, 2006, **2**, 8-21.
32. T. Govender, S. Stolnik, M. C. Garnett, L. Illum and S. S. Davis, *J. Control. Release*, 1999, **57**, 171-185.
33. T. Govender, T. Riley, T. Ehtezazi, M. C. Garnett, S. Stolnik, L. Illum and S. S. Davis, *Int. J. Pharm.*, 2000, **199**, 95-110.
34. C. Deng, Y. Jiang, R. Cheng, F. Meng and Z. Zhong, *Nano Today*, 2012, **7**, 467-480.
35. F. Meng, R. Cheng, C. Deng and Z. Zhong, *Materials Today*, 2012, **15**, 436-442.
36. M. L. Hans and A. M. Lowman, *Curr Opin Solid St M*, 2002, **6**, 319-327.

37. J. Lim, A. Chouai, S.-T. Lo, W. Liu, X. Sun and E. E. Simanek, *Bioconjug. Chem.*, 2009, **20**, 2154-2161.
38. K. S. Soppimath, T. M. Aminabhavi, A. R. Kulkarni and W. E. Rudzinski, *J. Control. Release*, 2001, **70**, 1-20.
39. D. Shenoy, S. Little, R. Langer and M. Amiji, *Pharm. Res.*, 2005, **22**, 2107-2114.
40. V. P. Torchilin, *The AAPS Journal*, 2007, **9**, E128-E147.
41. D. Shenoy, S. Little, R. Langer and M. Amiji, *Mol. Pharm.*, 2005, **2**, 357-366.
42. S. Kommareddy and M. Amiji, *Bioconjug. Chem.*, 2005, **16**, 1423-1432.
43. I. Lentacker, R. E. Vandenbroucke, B. Lucas, J. Demeester, S. C. De Smedt and N. N. Sanders, *J. Control. Release*, 2008, **132**, 279-288.
44. P. Vaupel, F. Kallinowski and P. Okunieff, *Cancer Res*, 1989, **49**, 6449-6465.
45. J.-K. Kim, V. K. Garripelli, U.-H. Jeong, J.-S. Park, M. A. Repka and S. Jo, *Int. J. Pharm.*, 2010, **401**, 79-86.
46. S. Binauld, W. Scarano and M. H. Stenzel, *Macromolecules*, 2012, **45**, 6989-6999.
47. T. Etrych, M. Sirova, L. Starovoytova, B. Rihova and K. Ulbrich, *Mol. Pharmaceutics*, 2010, **7**, 1015-1026.
48. A. K. Pearce, B. E. Rolfe, P. J. Russell, B. W. C. Tse, A. K. Whittaker, A. V. Fuchs and K. J. Thurecht, *Polymer Chemistry*, 2014, **5**, 6932-6942.
49. D. M. Euhus, C. Hudd, M. C. Laregina and F. E. Johnson, *J. Surg. Oncol.*, 1986, **31**, 229-234.
50. L. M. Kaminskas, V. M. McLeod, B. D. Kelly, C. Cullinane, G. Sberna, M. Williamson, B. J. Boyd, D. J. Owen and C. J. Porter, *Mol. Pharm.*, 2012, **9**, 422-432.
51. M. Wartenberg, J. Hescheler, H. Acker, H. Diedershagen and H. Sauer, *Cytometry*, 1998, **31**, 137-145.
52. B. Elsadek, R. Graeser, N. Esser, C. Schafer-Obodozie, C. Tsurumi, K. Abu Ajaj, A. Warnecke, C. Unger, T. Saleem and F. Kratz, *Prostate Cancer Prostatic Dis*, 2011, **14**, 14-21.
53. H. Jung, S. A. Kim, E. Lee and H. Mok, *Macromol. Res.*, 2015, **23**, 449-456.
54. W. L. Ye, Y. P. Zhao, R. Na, F. Li, Q. B. Mei, M. G. Zhao and S. Y. Zhou, *J. Pharm. Sci.*, 2015, **104**, 2293-2303.
55. T. Etrych, M. Jelinkova, B. Rihova and K. Ulbrich, *J. Control. Release*, 2001, **73**, 89-102.
56. M. Longmire, P. L. Choyke and H. Kobayashi, *Nanomed.*, 2008, **3**, 703-717.
57. H. S. Choi, W. Liu, P. Misra, E. Tanaka, J. P. Zimmer, B. I. Ipe, M. G. Bawendi and J. V. Frangioni, *Nat. Biotechnol.*, 2007, **25**, 1165-1170.
58. G. Minotti, P. Menna, E. Salvatorelli, G. Cairo and L. Gianni, *Pharmacol. Rev.*, 2004, **56**, 185-229.
59. X. Peng, B. Chen, C. C. Lim and D. B. Sawyer, *Mol. Interv.*, 2005, **5**, 163-171.
60. Y. Matsumura, T. Hamaguchi, T. Ura, K. Muro, Y. Yamada, Y. Shimada, K. Shirao, T. Okusaka, H. Ueno and M. Ikeda, *Br. J. Cancer*, 2004, **91**, 1775-1781.
61. T. Nakanishi, S. Fukushima, K. Okamoto, M. Suzuki, Y. Matsumura, M. Yokoyama, T. Okano, Y. Sakurai and K. Kataoka, *J. Control. Release*, 2001, **74**, 295-302.
62. L. M. Kaminskas, V. M. McLeod, B. D. Kelly, G. Sberna, B. J. Boyd, M. Williamson, D. J. Owen and C. J. Porter, *Nanomedicine: Nanotechnology, Biology and Medicine*, 2012, **8**, 103-111.
63. H. Maeda, G. Y. Bharate and J. Daruwalla, *Eur. J. Pharm. Biopharm.*, 2009, **71**, 409-419.